Direct determination of the number-weighted mean radius and polydispersity from dynamic light-scattering data

Philipus J. Patty and Barbara J. Frisken

We compare results for the number-weighted mean radius and polydispersity obtained either by directly fitting number distributions to dynamic light-scattering data or by converting results obtained by fitting intensity-weighted distributions. We find that results from fits using number distributions are angle independent and that converting intensity-weighted distributions is not always reliable, especially when the polydispersity of the sample is large. We compare the results of fitting symmetric and asymmetric distributions, as represented by Gaussian and Schulz distributions, respectively, to data for extruded vesicles and find that the Schulz distribution provides a better estimate of the size distribution for these samples.

OCIS codes: 290.0290, 290.5850.

1. Introduction

Dynamic light-scattering (DLS) techniques are frequently used to estimate particle-size distributions.[1,2] In these measurements the intensity of light scattered from a particle dispersion is detected and the intensity–intensity autocorrelation function of the light is calculated. In most cases this is related to the field–field autocorrelation function. For monodisperse particle dispersions, the field–field autocorrelation function decays exponentially with a decay rate proportional to the diffusion coefficient of the particles. If the sample is polydisperse, the field–field correlation function consists of a distribution of decay rates. In this case the correlation function data are usually analyzed in terms of the moments or cumulants of the decay rate distribution.[3,4] Alternatively, the decay rate distribution is determined by direct numerical inversion of DLS data by using a regularized Laplace inversion such as Contin.[5,6] The mean and standard deviation of the decay rate distribution can be determined by either method, from which the hydrodynamic radius and relative standard deviation are calculated.

Because the scattered intensity is weighted by both the mass and the form factor of the scattering objects, the hydrodynamic radius determined by these techniques can depend on the angle at which the scattered intensity is measured. This effect is significant for larger, more polydisperse particles. To overcome this problem, we must determine the number-weighted distribution, which is scattering-angle independent.

One example of particles that are frequently investigated using light scattering are extruded vesicles. Studies reveal them to be a prototypical example of polydisperse, spherical particles. The size distribution of the extruded vesicles has been characterized by different methods such as freeze-fracture electron microscopy,[7,8] cryogenic transmission electron microscopy,[9,10] field flow fractionation,[11] and static light scattering.[12,13] In particular, DLS has been used extensively because sample preparation is simple, the measurement is noninvasive, and the measurement time is relatively short compared with other methods, including static light scattering.[14–18] Detailed studies show that vesicles range in size from tens to hundreds of nanometers, depending on the size of the polycarbonate membrane filters and the pressure used during extrusion, and that they have polydispersities of 20%–30%.[7,19] If they are made in pure water, they are also spherical.[8]

There are a few groups that directly determine

The authors are with the Department of Physics, Simon Fraser University, Burnaby, British Columbia V5A 1S6, Canada. B. J. Frisken's e-mail address is frisken@sfu.ca.

Received 4 November 2005; revised 30 November 2005; accepted 30 November 2005; posted 1 December 2005 (Doc. ID 65756).

0003-6935/06/102209-08$15.00/0

number-weighted distributions of extruded vesicles. A number-weighted distribution of arbitrary functionality can be obtained by using discrete Laplace inversion algorithms.[20] Alternatively, number-weighted distributions have been determined by multiangle DLS measurements;[21] this requires long measurement times, especially when large vesicles and small angles are involved.

A more common approach is to attempt to convert the results of either cumulants analysis or an intensity-weighted distribution to a number-weighted radius distribution. Results from cumulants analysis have been converted to number distributions that have the form of a log-normal distribution,[22,23] a Gaussian or normal distribution,[24] a Schulz distribution,[22,25,26] or even an arbitrary distribution function.[27] These methods are based on the assumption that particles are small such that the form factor is equal to 1. In fact, this assumption is not valid in many measurements involving large particles. The form factor can be included in the conversion of intensity-weighted distributions to number distributions.[28]

In these studies we investigate the determination of number-weighted mean radius and polydispersity from DLS data by using nonlinear least-squares fitting methods to directly fit the distribution to the data. DLS measurements of the light scattered by extruded vesicles were made over a wide range of scattering angles. Various distributions were fit to the data, and the scattering-angle dependence and robustness of the results were compared. In particular, two functional forms for the vesicle radius distribution, Gaussian and Schulz, were investigated to show the effect of the symmetry of the distribution on the results. The results for the mean radius and the polydispersity obtained by direct fitting of a number-distribution to the data were compared with the results calculated from the determination of the intensity-weighted radius distribution.

2. Radius Distributions by Dynamic Light Scattering

A. Types of Distributions

Gaussian and Schulz distributions are used in these studies to represent symmetric and asymmetric distributions, respectively. The Gaussian distribution is written as

$$G(R) = \left(\frac{1}{\sqrt{2\pi}s}\right)\exp\left[\frac{-(\overline{R}-R)^2}{2s^2}\right], \quad (1)$$

where $\overline{R}$ and s are the mean radius and standard deviation, respectively. We define polydispersity as the relative standard deviation, $\sigma = s/\overline{R}$. The Schulz distribution, on the other hand, is written as

$$G(R) = \left(\frac{m+1}{\overline{R}}\right)^{m+1}\frac{R^m}{m!}\exp\left[\frac{-R(m+1)}{\overline{R}}\right], \quad (2)$$

where $\sigma^2 = 1/(m+1)$.

B. Intensity-Weighted Distribution

The quantity measured in DLS is the intensity–intensity autocorrelation function $g^2(\tau)$. In most cases this function can be written in terms of the field–field autocorrelation function $g^{(1)}(\tau)$ through the Siegert relation[1,2]

$$g^{(2)}(\tau) = B + \beta[g^{(1)}(\tau)]^2, \quad (3)$$

where τ is the delay time and β is a factor that depends on the experimental geometry. At long delay times, the correlation function decays to a baseline value B, which should be very close to 1.

For monodisperse particles undergoing Brownian motion, the field–field autocorrelation function decays exponentially as follows:

$$g^{(1)}(\tau) = \exp[-\Gamma\tau], \quad (4)$$

with a decay rate $\Gamma = Dq^2$ that depends on the diffusion coefficient of the particles D and on the magnitude of the scattering wave vector $q = (4\pi n/\lambda)\sin(\theta/2)$, where λ is the wavelength of the light source in vacuum, n is the refractive index of the medium, and θ is the scattering angle. The hydrodynamic radius can then be determined by using the Stokes–Einstein relation:

$$R_h = \frac{k_B T}{6\pi\eta D} = \frac{k_B T q^2}{6\pi\eta\Gamma}, \quad (5)$$

where k_B is Boltzmann's constant, T is the temperature, and η is the viscosity of the dispersant.

For polydisperse particles, there will be a distribution of decay rates instead of a single decay rate. In this case $g^{(1)}(\tau)$ is given by

$$g^{(1)}(\tau) = \int_0^\infty G(\Gamma)\exp[-\Gamma\tau]d\Gamma, \quad (6)$$

where $G(\Gamma)$ describes the distribution of decay rates and is normalized. $G(\Gamma)$ is characterized by a mean decay rate

$$\overline{\Gamma} = \int_0^\infty \Gamma\, G(\Gamma)d\Gamma \quad (7)$$

and a relative variance

$$\frac{s_\Gamma{}^2}{\overline{\Gamma}^2} = \int_0^\infty \frac{(\Gamma-\overline{\Gamma})^2}{\overline{\Gamma}^2} G(\Gamma)d\Gamma. \quad (8)$$

After assuming a functional form for $G(\Gamma)$, we can fit Eq. (3) to the intensity–intensity autocorrelation function data by using Eq. (6) for the field–field autocorrelation function. Then $\bar{\Gamma}$ and associated polydispersity σ_Γ can be determined by applying Eqs. (7) and (8).

Alternatively, in a moments-based analysis, $g^{(1)}(\tau)$ is expanded in terms of the moments of the distribution[3,4]

$$g^{(1)}(\tau) = \exp\left[-\bar{\Gamma}\tau\right]\left(1 + \frac{\mu_2}{2!}\tau_2 - \frac{\mu_2}{3!}\tau_3 + \cdots\right), \quad (9)$$

where μ_n are the moments of the distribution and, in particular, $\mu_2 = s_\Gamma{}^2$ and μ_3 represent the variance and skewness of the distribution, respectively. Γ and $\sigma_\Gamma = s_\Gamma/\bar{\Gamma}$ can be determined directly by fitting Eq. (3) to the intensity–intensity autocorrelation function data by using Eq. (9) for the field–field autocorrelation function.

After the decay rate distribution has been determined, the particle size and size distribution can be estimated. The hydrodynamic radius R_h is calculated by using $\bar{\Gamma}$ and Eq. (5). In these methods the relative variance of R_h is generally assumed to be equal to the relative variance of Γ.

Instead of working with a decay rate distribution, we can reformulate the analysis in terms of a radius distribution. Equation (6) can be written in terms of an intensity-weighted radius distribution $G_i(R)$ by using Eq. (5):

$$g^{(1)}(\tau) = \int_0^\infty G_i(R)\exp\left[\frac{-k_B T q^2}{6\pi\eta R}\tau\right]\mathrm{d}R, \quad (10)$$

where $G_i(R)\mathrm{d}R = G(\Gamma)\mathrm{d}\Gamma$ and $G_i(R)$ is normalized. The intensity-weighted mean radius R_i and polydispersity σ_{R_i} can be determined by applying the results for $G_i(R)$.

C. Number-Weighted Distribution

In general, the scattered intensity is proportional to the square of the mass M of the particle so that each particle's contribution to the scattered intensity depends strongly on its size.[1] The scattered intensity also has an angular dependence due to interference effects that is represented by the form factor of the particles. This angular dependence becomes more pronounced for larger particles, with larger particles contributing more to the scattered intensity at small angles than at large angles. Consequently, R_h and R_i determined from $G(\Gamma)$ and $G_i(R)$, respectively, become angle dependent. To determine a size distribution that is independent of angle, we should include M^2 and the form factor in the analysis.

For vesicles, the form factor can be written as[15]

$$F(R) = \left[\frac{\sin(qR)}{qR}\right]^2, \quad (11)$$

and M^2 is proportional to R^4. The expression for $g^{(1)}(\tau)$ in terms of the number-weighted distribution $G_n(R)$ is then written as

$$g^{(1)}(\tau) = \frac{\int_0^\infty G_n(R)R^4F(R)\exp\left[\left(-k_BTq^2/6\pi\eta R\right)\tau\right]\mathrm{d}R}{\int_0^\infty G_n(R)R^4F(R)\mathrm{d}R}. \quad (12)$$

The number-weighted mean radius and polydispersity can be determined directly by fitting Eq. (3) to the intensity–intensity autocorrelation function data by using Eq. (12) for $g^{(1)}(\tau)$ with an appropriate functional form of $G_n(R)$.

D. Relation between $G_i(R)$ and $G_n(R)$

The number-weighted distribution $G_n(R)$ can be written in terms of the intensity-weighted distribution $G_i(R)$ as[28]

$$G_n(R) = A\frac{G_i(R)}{R^4F(R)}, \quad (13)$$

where

$$A = \left[\int_0^\infty \frac{G_i(R)}{R^4F(R)}\,\mathrm{d}R\right]^{-1} \quad (14)$$

has been introduced so that $G_n(R)$ is normalized.

The mean radius and polydispersity of the number-weighted distribution $G_n(R)$ can then be calculated from the intensity-weighted distributions by using Eq. (13).

E. Relation between R_h and the Number-Weighted Distribution

From the Stokes–Einstein relation, Eq. (5), the hydrodynamic radius can be written as

$$R_h = \frac{k_BTq^2}{6\pi\eta}\frac{1}{\bar{\Gamma}} = \frac{k_BTq^2}{6\pi\eta}\frac{1}{\overline{R^{-1}}}. \quad (15)$$

The hydrodynamic radius and associated polydispersity σ_{R_h} can then be calculated from the number distribution $G_n(R)$,

$$R_h = \frac{\int_0^\infty G_n(R)R^4F(R)\mathrm{d}R}{\int_0^\infty R^{-1}G_n(R)R^4F(R)\mathrm{d}R} = \frac{\int_0^\infty G_n(R)R^4F(R)\mathrm{d}R}{\int_0^\infty G_n(R)R^3F(R)\mathrm{d}R}, \tag{16}$$

$$\sigma_{R_n}{}^2 = \frac{\int_0^\infty G_n(R)R^4F(R)\mathrm{d}R\int_0^\infty R^2G_n(R)F(R)\mathrm{d}R}{\left[\int_0^\infty R^3G_n(R)F(R)\mathrm{d}R\right]^2} - 1. \tag{17}$$

3. Materials and Methods

The method that we use to prepare vesicles was described previously.[29] The lipid used in these studies was 1-stearoyl-2-oleoyl-*sn*-glycero-3-phosphatidylcholine (SOPC); it was purchased from Avanti Polar Lipids (Birmingham, Alabama). The vesicles were prepared by hydrating SOPC in purified water from a Milli-Q plus water purification system (Millipore, Bedford, Massachusetts). The use of purified water ensures the production of spherical vesicles.[8] The hydrated sample was taken through a freeze–thaw–vortex process and pre-extruded through two 400 nm diameter polycarbonate track etch (PCTE), membranes. The pre-extruded samples were then extruded through PCTEs with nominal pore radii of 50 and 100 nm. For the rest of the paper, vesicles produced using these pore sizes are defined as 50 and 100 nm vesicles, respectively. DLS measurements were performed on samples consisting of a ratio of 0.1 mg lipid to 1 ml water.

An ALV DLS/SLS-5000 spectrometer/goniometer manufactured by ALV-Laser GmbH (Langen, Germany) and a HeNe laser ($\lambda = 633$ nm) were used for these experiments. The ALV correlator features 288 logarithmically spaced delay times ranging from 200 ns to 1 s. Samples were measured at scattering angles ranging from 20° to 150°. Five measurements were made at each angle.

Fits to the data were made using weighted nonlinear least-squares fitting routines. In general, no significant difference in the goodness-of-fit parameter or the residuals was observed either when the two different distributions, Schulz and Gaussian, were used or when fits made using intensity-weighted distributions were compared with number-weighted distributions in fits of the same data. The baseline B was a parameter in each fit; the other parameters were β and the parameters describing the distribution.

4. Results and Discussion

Intensity correlation functions calculated for each measurement were analyzed by fitting Eq. (3) and one of four different forms of the field-correlation function $g^{(1)}(\tau)$, Eqs. (6), (9), (10), and (12) to the data.

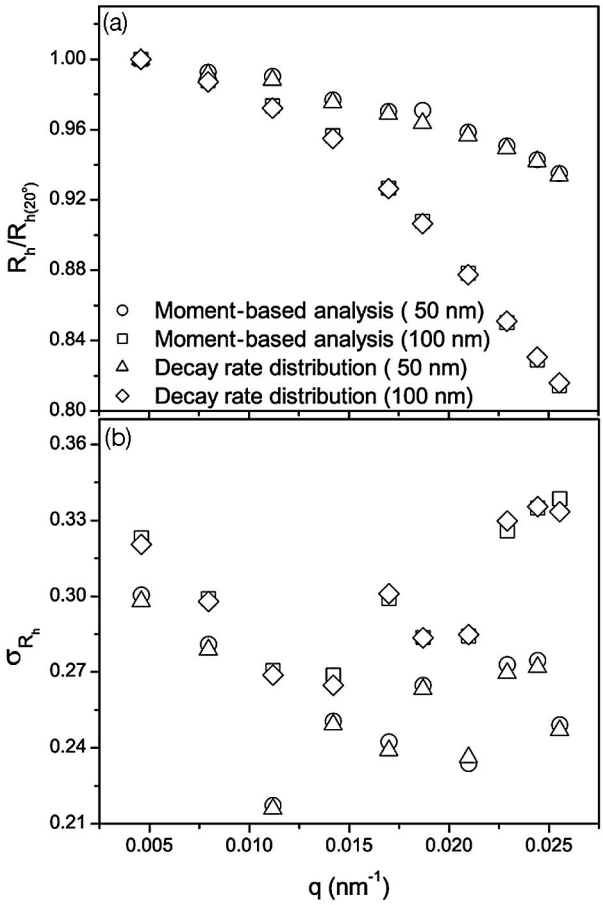

Fig. 1. (a) Hydrodynamic radius normalized by the radius measured at 20° and (b) polydispersity of 50 and 100 nm vesicles as a function of q. The results were determined by using $g^{(1)}(\tau)$, consisting of either a decay rate distribution [Eq. (6)] or a moments-based analysis [Eq. (9)].

First we determined the results for the decay rate distributions. We fit a model function based on the expansion of the correlation function in terms of the moments of the decay rate distribution [Eq. (9)] to the data. In general, it was found to be necessary to fit Eq. (9) only up to the second order. We then assumed a Gaussian distribution and fit a model function based on a correlation function as given by Eq. (6) to the data. The mean decay rate and polydispersity ($\bar{\Gamma}$ and σ_Γ, respectively) were determined from these fits, and the hydrodynamic radius R_h and polydispersity σ_{R_h} were calculated. The results for the hydrodynamic radius R_h and the polydispersity σ_{R_h} as a function of q for 50 and 100 nm vesicles are shown in Figs. 1(a) and 1(b), respectively. Here R_h was normalized to the value of R_h at 20° to allow comparison of the q dependence of the hydrodynamic radius calculated for 50 and 100 nm vesicles. The results from both approaches are consistent: R_h decreases with increasing q, and the q dependence is more pronounced for the larger vesicles. The mean radius of the larger vesicles decreases by 20% over the angular

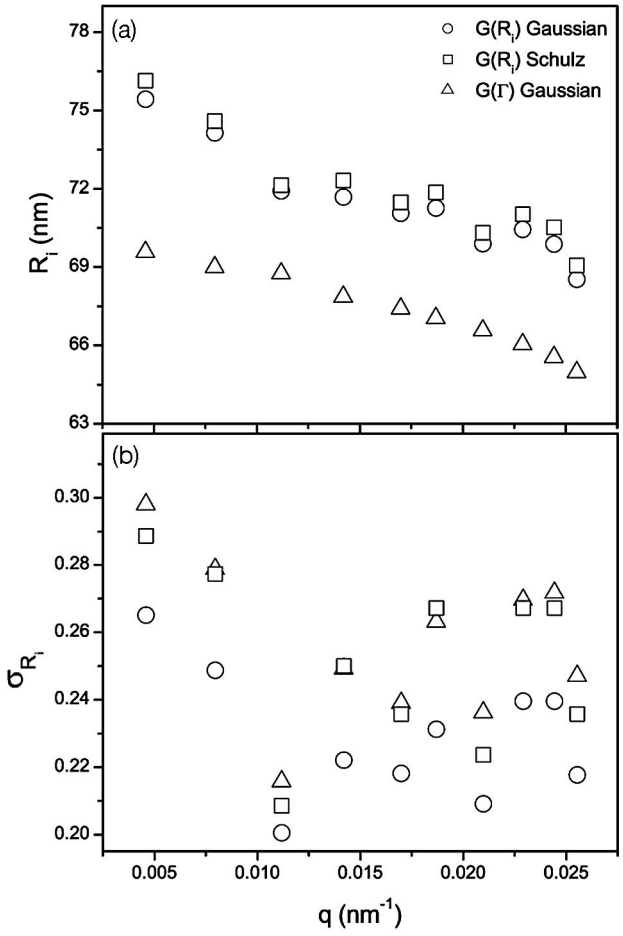

Fig. 2. (a) Intensity-weighted mean radius R_i and (b) polydispersity σ_{R_i} *of* 50 nm vesicles as a function of q. The results were determined by using $g^{(1)}(\tau)$, expressed in terms of the intensity-weighted radius distribution $G_i(R)$ [Eq. (10)], in which Gaussian and Schulz distributions were used for $G_i(R)$. For comparison, the results for 50 nm vesicles from Fig. 1 are also shown.

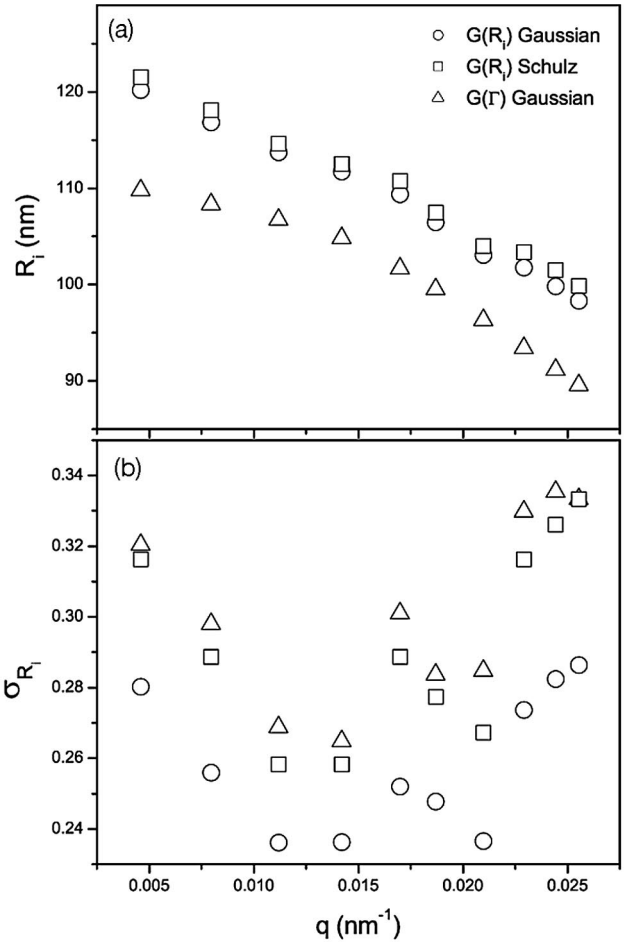

Fig. 3. (a) Intensity-weighted mean radius R_i and (b) polydispersity σ_{R_i} of 100 nm vesicles as a function of q. The results were determined by using $g^{(1)}(\tau)$, expressed in terms of the intensity-weighted radius distribution $G_i(R)$ [Eq. (10)], in which Gaussian and Schulz distributions were used for $G_i(R)$. For comparison, the results for 100 nm vesicles from Fig. 1 are also shown.

range measured in these experiments. The results for σ_{R_h} do not indicate any particular q dependence.

The intensity-weighted mean radius R_i and polydispersity σ_{R_i} were determined from the results of fitting with Eq. (10). Figures 2 and 3 show (a) the intensity-weighted mean radius R_i and (b) the polydispersity σ_{R_i} as a function of q for 50 and 100 nm vesicles, respectively. The results for R_h and σ_{R_h} determined by using $g^{(1)}(\tau)$ expressed in terms of the Gaussian decay rate distribution are also shown for comparison. As expected, the intensity-weighted mean radius also decreases as q increases, with the q dependence more pronounced for larger vesicles. There is a significant difference between the mean radius and the polydispersity found using the decay rate and radius distributions in $g^{(1)}(\tau)$. This reflects the fact that these are actually different averages; R_i is obtained by averaging over R while R_h is obtained by averaging over R^{-1}. R_i is larger than R_h for both Gaussian and Schulz distributions, where as the Gaussian R_i is slightly smaller than the Schulz R_i. On the other hand, the Schulz σ_{R_i} is similar to σ_{R_h}, while the Gaussian σ_{R_i} is systematically smaller than both the Schulz σ_{R_i} and σ_{R_h}.

The number-weighted mean radius R_n and polydispersity σ_{R_n} were first determined from the results of fitting with Eq. (12). Figures 4 and 5 show (a) the number-weighted mean radius R_n and (b) the polydispersity σ_{R_n} as a function of q for 50 and 100 nm vesicles, respectively. The number-weighted mean radius and polydispersity can be determined by directly fitting the data, although the results from fitting the Schulz distribution to the data are significantly better. With the exception of the data taken at the smallest q, there is no significant q dependence for R_n and σ_{R_n} determined by using the Schulz distribution, and the values obtained for the polydispersity are reasonable. However, when the Gaussian distribution is used, more q dependence is observed in the results for R_n, especially for the larger vesicles. Values for R_n are low for both distributions at the smallest q measured. This is not surprising, as DLS measurements at low q are very sensitive to dust or aggregates in the sample. Neither

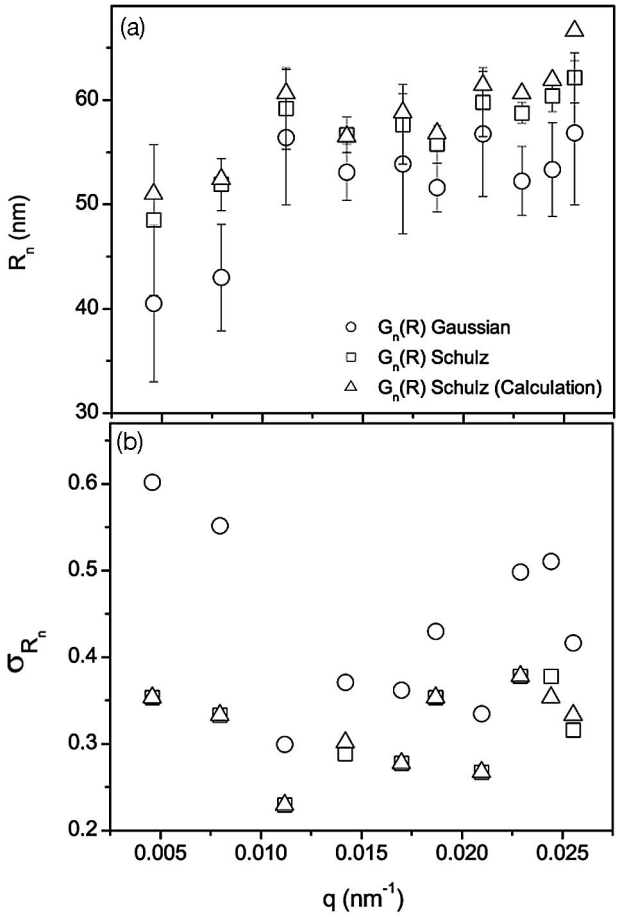

Fig. 4. (a) Number-weighted mean radius R_n and (b) polydispersity σ_{R_n} of 50 nm vesicles as a function of q. The results were determined by using $g^{(1)}(\tau)$ expressed in terms of the number-weighted radius distribution $G_n(R)$ [Eq. (12)], in which Gaussian and Schulz distribution were used for $G_n(R)$. For comparison, R_n and σ_{R_n}, calculated using Eq. (13) and fit results for R_i and σ_{R_i} as shown in Fig. 2, are also shown. The error bars represent the standard deviation of the mean value from five measurements.

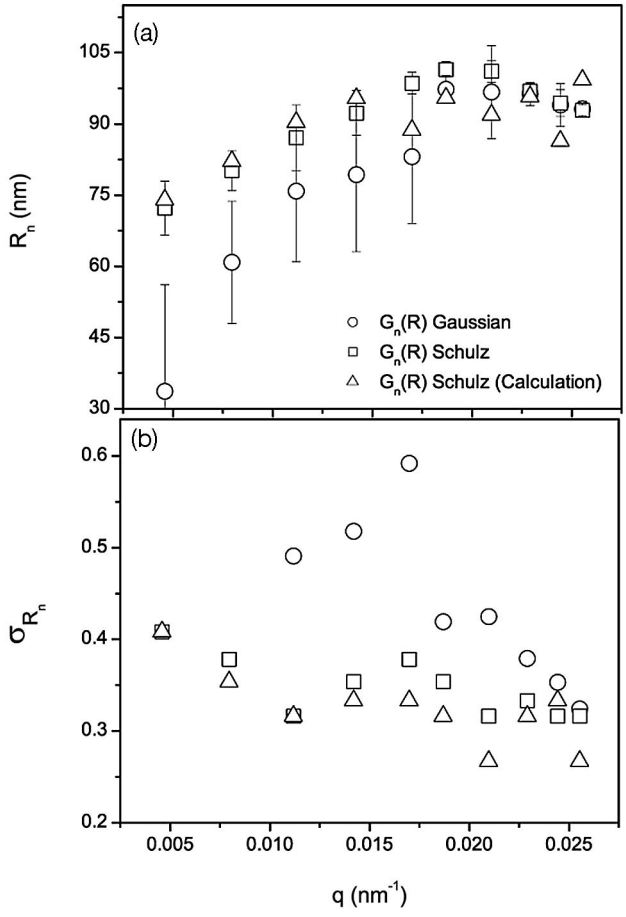

Fig. 5. (a) Number-weighted mean radius R_n and (b) polydispersity σ_{R_n} of 100 nm vesicles as a function of q. The results were determined using $g^{(1)}(\tau)$ expressed in terms of the number-weighted radius distribution $G_n(R)$ [Eq. (12)] in which Gaussian and Schulz distributions were used for $G_n(R)$. For comparison, R_n and σ_{R_n}, calculated using Eq. (13) and fit results for R_i and σ_{R_i} shown in Fig. 2, are also shown. The error bars represent the standard deviation of the mean value from five measurements.

would be accounted for in these distributions, which are monomodal. There is a significant difference in the values found for R_n and σ_{R_n}, depending on whether the Gaussian or Schulz distribution is used. The mean radius found using the Schulz distribution is larger than that found using the Gaussian distribution. The value of σ_{R_n} from the Gaussian distribution, however, is very large, particularly at small q. The fact that the Schulz distribution does a better job of fitting data for extruded vesicles is consistent with the findings of other authors.[20]

Next we tested whether the results obtained for intensity-weighted distributions can be used to calculate number-averaged results for R_n and σ_{R_n}. The mean radius and polydispersity R_n and σ_{R_n} were calculated by using a number distribution given by Eq. (13), with intensity-weighted distributions determined by fits to the data. Only the results for the Schulz distribution are shown in Figs. 4 and 5 for 50 and 100 nm vesicles, respectively. For this case, calculated R_n and σ_{R_n} agree well with the results from direct fitting of the number-weighted distribution to the data. However, the results for the Gaussian distribution are not shown because the results calculated for R_n and σ_{R_n} are significantly different from the results of the direct fit of the number distribution to the data; the results for R_n are much too small, and those for σ_{R_n} are much too large.

One possible source for the failure of the conversion from an intensity-weighted Gaussian distribution to a number-weighted distribution is the polydispersity of these samples. This can be confirmed by calculating R_n and σ_{R_n} from R_i and σ_{R_i} respectively, by using Eq. (13) and a range of σ_{R_i}. Calculated results for R_n and σ_{R_n} for vesicles with R_i of 60 and 90 nm as a function of σ_{R_i} are shown in Figs. 6(a) and 6(b), respectively. The values chosen for R_i are close to those measured for 50 and 100 nm vesicles, respectively. In the graph the number-weighted values are normalized by the intensity-weighted values to make it easy to compare the results for 50 and 100 nm vesi-

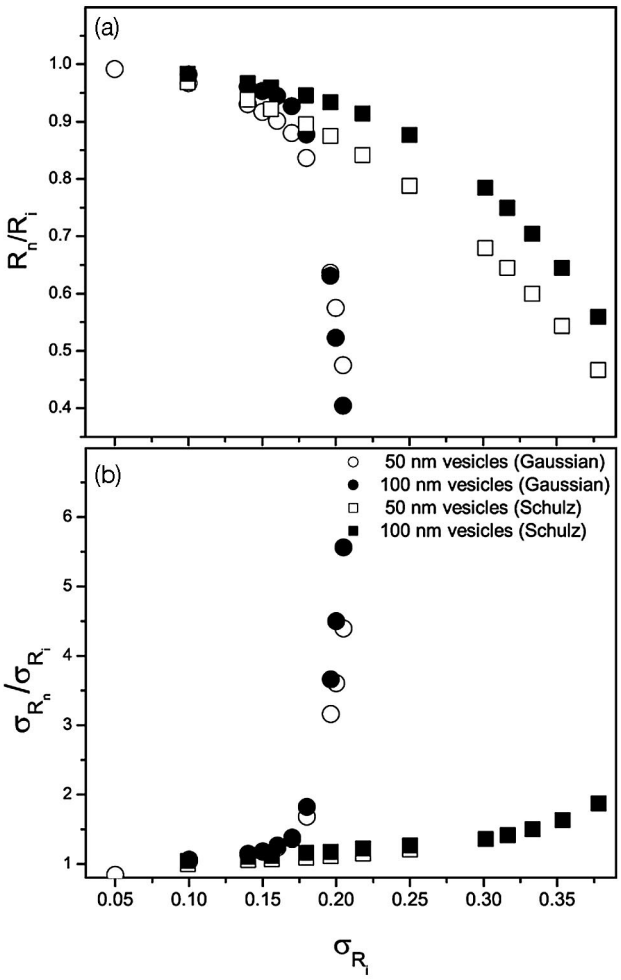

Fig. 6. Values for (a) R_n and (b) σ_{R_n} calculated as a function of σ_{R_i} of vesicles with R_i values of 60 and 90 nm by using Eq. (13) for both Gaussian and Schulz distributions of vesicles.

cles. When σ_{R_i} is small, R_n and σ_{R_n} are almost the same as R_i and σ_{R_i}, respectively. As σ_{R_i} increases, R_n becomes smaller than R_i, while σ_{R_n} becomes larger than σ_{R_i}. For σ_{R_i} larger than a certain threshold value, R_n becomes very small, while σ_{R_n} becomes very large. In this case the threshold value above which the difference between the two results is unacceptable is much smaller for the Gaussian distribution (approximately 0.15) than it is for the Schultz distribution (approximately 0.30). As the polydispersity observed in these samples is >0.15, the conversion from an intensity-weighted Gaussian distribution to a number-weighted distribution yields unreasonable values.

5. Conclusions

In this paper we have demonstrated an approach that can be used to determine the number-weighted mean radius and the polydispersity directly from DLS data. By fitting number-weighted radius distributions, and including the mass and form factor in the fitting, the apparent problem of q dependence of DLS-measured particle size can be overcome. We have also shown that results obtained by using an intensity-weighted distribution should be converted to number-weighted results with care, especially if the polydispersity is large. We have shown this by using nonlinear least-squares fitting techniques to fit a correlation function that is calculated by numerical integration over the product of a number distribution of the radii, the particle form factor, the square of the mass, and the exponential decay factor. Alternatively, one could incorporate information about particle shape and scattering into Contin or nonnegative least-squares fitting method.

We have applied this technique to measurements of extruded vesicles. In particular, we have used Gaussian and Schulz distributions, representing symmetric and asymmetric distributions, respectively, to determine the mean radius and the polydispersity for vesicles extruded through 50 and 100 nm pores. The q dependence of the radius determined by using a number-weighted distribution was found to be minimal for 50 and 100 nm vesicles when a Schulz distribution was used but was acceptable only for 50 nm vesicles when the Gaussian distribution was used. The results are also consistent with the size distribution of extruded vesicles' being asymmetric.

The authors gratefully acknowledge the financial support of the Natural Sciences and Engineering Research Council of Canada.

References

1. B. J. Berne and R. Pecora, *Dynamic Light Scattering with Applications to Chemistry, Biology and Physics* (Robert E. Krieger, 1990).
2. P. Štěpánek, "Data analysis in dynamic light scattering," in *Dynamic Light Scattering: the Method and Some Applications,* W. Brown, ed. (Oxford U. Press, 1993), pp. 177–241.
3. D. E. Koppel, "Analysis of macromolecular polydispersity in intensity autocorrelation spectroscopy: the method of cumulants," J. Chem. Phys. **57,** 4814–4820 (1972).
4. B. J. Frisken, "Revisiting the method of cumulants for analysis dynamic light scattering data," J. Appl. Opt. **40,** 4087–4091 (2001).
5. S. Provencher, "Contin: a general purpose constrained regularization program for inverting noise linear algebraic and integral equations," Comp. Phys. Commun. **27,** 229–242 (1982).
6. S. Provencher, "A constrained regularization method for inverting data represented by linear algebraic or integral equations," Comp. Phys. Commun. **27,** 213–227 (1982).
7. L. D. Mayer, M. J. Hope, and P. R. Cullis, "Vesicles of variable sizes produced by a rapid extrusion procedure," Biochim. Biophys. Acta **858,** 161–168 (1986).
8. B. Mui, P. R. Cullis, E. Evans, and T. D. Madden, "Osmotic properties of large unilamellar vesicles prepared by extrusion," Biophys. J. **64,** 443–453 (1993).
9. Y. Talmon, J. L. Burns, M. H. Chesnut, and D. P. Siegel, "Time-resolved cryotransmission electron microscopy," J. Electron Microsc. Tech. **14,** 6–12 (1990).
10. M. Almgren, K. Edwards, and G. Karlsson, "Cryotransmission electron microscopy of liposomes and related structures," Colloid. Surf. A **174,** 3–21 (2000).
11. B. A. Korgel, J. H. van Zanten, and H. G. Monbouquette, "Vesicle size distribution measured by field-flow-fractionation

coupled with multiangle light scattering," Biophys. J. **74,** 3264–3272 (1998).
12. J. H. van Zanten and H. G. Monbouquette, "Characterization of vesicles by classical light scattering," J. Colloid Interface Sci. **146,** 330–336 (1991).
13. J. H. van Zanten and H. G. Monbouquette, "Phosphatidylcholine vesicle diameter, molecular weight and wall thickness determined by static light-scattering," J. Colloid Interface Sci. **165,** 512–518 (1994).
14. J. C. Selser and R. J. Baskin, "A light scattering characterization of membrane vesicles," Biophys. J. **16,** 337–356 (1976).
15. F. R. Hallett, J. Watton, and P. Krygsman, "Vesicle sizing-number distribution by dynamic light scattering," Biophys. J. **59,** 357–362 (1991).
16. S. Kölchens, V. Ramaswami, J. Birgenheier, L. Nett, and D. F. O'Brien, "Quasi-elastic light scattering determination of the size distribution of extruded vesicles," Chem. Phys. Lipids **65,** 1–10 (1993).
17. A. J. Jin, D. Huster, and K. Gawrisch, "Light scattering characterization of extruded lipid vesicles," Eur. Biophys. J. **28,** 187–199 (1999).
18. B. J. Frisken, C. Asman, and P. J. Patty, "Studies of vesicle extrusion," Langmuir **16,** 928–933 (2000).
19. P. J. Patty and B. J. Frisken, "The pressure-dependence of the size of extruded vesicles," Biophys. J. **85,** 996–1004 (2003).
20. F. R. Hallett, T. Craig, J. Marsh, and B. Nickel, "Particle size analysis: number distributions by dynamic light scattering," Can. J. Spectrosc. **34,** 63–70 (1989).
21. G. Bryant, C. Abeynayake, and J. C. Thomas, "Improve particle size distribution measurements using multiangle dynamic light scattering. 2. Refinements and applications," Langmuir **12,** 6224–6228 (1996).
22. L. H. Hanus and H. J. Ploehn, "Conversion of intensity-average photon correlation spectroscopy measurements to number-average particles size distributions. 1. Theoretical development," Langmuir **15,** 3091–3100 (1999).
23. J. C. Thomas, "The determination of log normal particle size distributions by dynamic light scattering," J. Colloid Interface Sci. **117,** 187–192 (1987).
24. C. B. Bargeron, "Measurements of continuous distribution of spherical particles by intensity correlation spectroscopy: analysis by cumulants," J. Chem. Phys. **61,** 2134–2138 (1974).
25. D. S. Horne, "Determination of the size distribution of bovine casein micelles using photon correlation spectroscopy," J. Colloid Interface Sci. **98,** 537–548 (1984).
26. T. W. Taylor, S. M. Scrivner, C. M. Sorensen, and J. F. Merklin, "Determination of the relative number distribution of particle sizes using photon correlation spectroscopy," Appl. Opt. **24,** 3713–3717 (1985).
27. J. C. Selser, "Letter: a light scattering method of measuring membrane vesicle-number average size and size dispersion," Biophys. J. **16,** 847–848 (1976).
28. J. Pencer and F. R. Hallett, "Effects of vesicle size and shape on static and dynamic light scattering measurements," Langmuir **19,** 7488–7497 (2003).
29. D. G. Hunter and B. J. Frisken, "The effects of lipid composition and extrusion pressure and temperature on the properties of phospholipid vesicles," Biophys. J. **74,** 2996–3000 (1998).